Available online at www.eccomasproceedia.org
Eccomas Proceedia COMPDYN (2025) 1773-1784

ECCOMAS
Proceedia

COMPDYN 2025
10th ECCOMAS Thematic Conference on
Computational Methods in Structural Dynamics and Earthquake Engineering
M. Papadrakakis, M. Fragiadakis (eds.)
Rhodes Island, Greece, 15-18 June 2025

# EXPERIMENTAL AND NUMERICAL ANALYSES OF A RESILIENT PRESTRESSED LEAD DAMPER

**Eleonora Bruschi[1], Virginio Quaglini[1], Carlo Pettorruso[1] and Gabriele Dubini[2]**

[1] Politecnico di Milano, Department of Architecture, Built Environment and Construction Engineering
Piazza Leonardo da Vinci 32, 20133 Milan, Italy
e-mail: {eleonora.bruschi, virginio.quaglini, carlo.pettorruso}@polimi.it

[2] Politecnico di Milano, Department of Chemistry, Materials and Chemical Engineering “Giulio Natta”
Piazza Leonardo da Vinci 32, 20133 Milan, Italy
gabriele.dubini@polimi.it

---

## Abstract

*This work presents an innovative hysteretic damper, named PreStressed LEad Damper (PS-LED) that dissipates seismic energy through the friction mechanism generated between a straight steel shaft and a lead core. A notable feature of the PS-LED is its capability to adjust the axial force by varying the prestress on the lead core, enabling the damper to accommodate specific design needs without modifying its physical dimensions, providing a significant advantage for serial production. This study outlines the conceptual framework of the PS-LED, highlighting its robust performance and durability during repeated loading cycles. An experimental campaign involving two prototypes is reported, validating the PS-LED's constitutive behavior and confirming the effectiveness of the design equations. Additionally, a numerical analysis is conducted on a 6-story reinforced concrete structure, retrofitted with diagonal steel braces equipped with either the PS-LED or a conventional Buckling Restrained Brace (BRB), to highlight the advantages of the PS-LED over the state-of-the-art device. Bidirectional non-linear dynamic analyses are conducted using natural ground motions selected from the European Ground Motion Database; the results demonstrate that the PS-LED significantly enhances energy dissipation capabilities, resulting in notable reductions in floor accelerations and shear forces impacting the columns of the structure when compared to the BRB. These outcomes underscore the PS-LED's potential to improve seismic resilience, presenting a viable alternative to traditional damping technologies.*

**Keywords:** Friction damper, Lead damper, Experimental study, Conceptual design, Nonlinear analyses, OpenSees

---


Peer-review under responsibility of the organizing committee of COMPDYN 2025.
doi: 10.7712/120125.12527.24458

# 1 INTRODUCTION

PS-LED, which stands for PreStressed LEad Damper is a novel energy dissipation device, which dissipates energy through the friction force activated from the movement of a steel shaft sliding inside a lead core [1]-[3], as illustrated in Figure 1(a). Figure 1(b) presents the theoretical force-displacement curve of the device, characterized by an elastic–perfectly plastic behavior typical of friction dampers. This leads to an almost perfectly rectangular hysteretic cycle, corresponding to a damping capacity significantly higher than that of Displacement Dependent Devices (DDDs) currently available on the market, and potentially reaching values ≥ 57%. Among DDDs, Buckling Restrained Braces (BRBs) represent the state of the art in steel hysteretic dampers and are widely adopted, as evidenced by extensive scientific literature (e.g., [4]-[15]) and numerous applications worldwide (e.g., [16]-[20]). BRBs typically achieve a damping capacity ranging from 30% to 40%, as reported by [21] and [22]. Therefore, the PS-LED surpasses BRBs in terms of energy dissipation capacity.

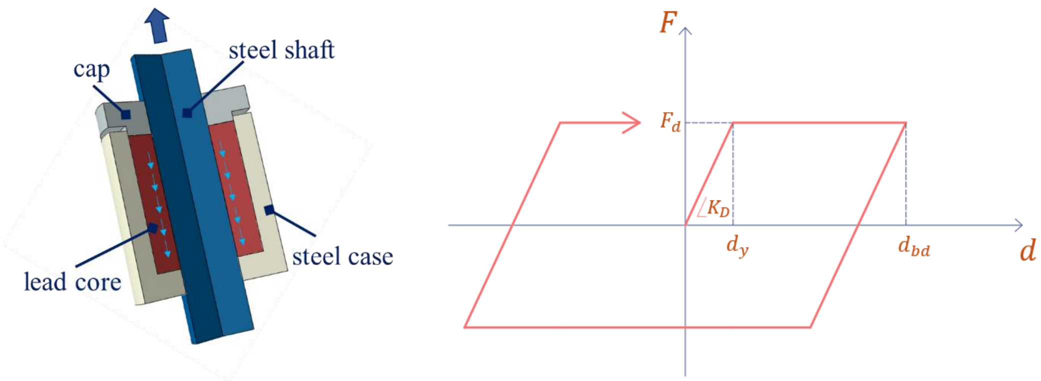


**Figure 1:** (a) Sketch and nomenclature of the main elements of the PS-LED; (b) theoretical force-displacement curve of the PS-LED

Furthermore, since the seismic energy in BRBs is dissipated primarily through the yielding of the steel core, they are prone to permanent deformations following an earthquake. This makes BRBs highly sensitive to low-cycle fatigue, necessitating their replacement after strong seismic events. Such replacements not only incur significant maintenance costs but also pose safety risks, as the structure remains vulnerable to aftershocks until the damaged dampers are replaced. In contrast, the PS-LED operates solely based on friction, ensuring that no mechanical components undergo plastic deformation or sustain damage. This design guarantees insensitivity to fatigue, enabling the device to withstand multiple design-level earthquakes without requiring maintenance [1]-[3].

In [2] a first prototype of the PS-LED was experimentally assessed following the testing protocol prescribed by the European norm on anti-seismic devices EN 15129 [23], referring to the category of DDDs, to which both PS-LED and BRB belong. This study provides insights into the conceptual development of the device and presents the outputs of the experimental campaign conducted on a second prototype. Additionally, the final section discusses numerical analyses performed on a case-study structure retrofitted with the PS-LED and subjected to a set of bidirectional natural ground motions. The effectiveness of the PS-LED retrofit strategy is assessed by comparing the structural performance of the retrofitted building with that of the same structure equipped with BRB, considered as the state of the art of the DDDs.

## 2 PS-LED: DESCRIPTION AND BASIC OPERATION PRINCIPLE

In its basic configuration, the PS-LED is made of a lead core confined into a rigid cylinder, with a steel shaft sliding inside the core under the applied force (Figure 1). One end of the cylinder is sealed with a solid plate, while the opposite end is enclosed by a container cap secured with screws. The core is composed of 99.99% pure lead, whereas the cylinder, shaft, and cap are made of structural steel. Additionally, the shaft is coated with hard chromium.

Starting from the unloaded condition, the first branch of the force-displacement curve, referring to displacements $d \leq d_y$, corresponds to the elastic deformation of the shaft under the applied force. At the yield displacement $d_y$, the force achieves the value $F_d$, which is equal to the friction force between the shaft and the core, as expressed in Eq.(1)

$$F_d = \tau \cdot (\pi D L_c) = \mu \cdot p_i \cdot (\pi D L_c) \tag{1}$$

where $D$ is the diameter of the shaft, $L_c$ is the axial length of the core (corresponding to the length of the core/shaft interface), and $\tau$ is the average shear stress, given by the product of the friction coefficient $\mu$ and the contact pressure at the shaft/core interface $p_i$. From this point on, an increase in displacement is accommodated by the shaft sliding inside the core, activating friction at the sliding interface, which dissipates energy. Since Eq.(1) is independent of the displacement of the shaft, the friction force remains constant, resulting in an almost rectangular hysteresis curve [2]. The theoretical energy dissipated in a fully reversed cycle of amplitude $d_{bd}$ is determined according to Eq.(2)

$$EDC = 4 \cdot F_d \cdot d_{bd} \tag{2}$$

The equivalent viscous damping ratio $\xi_{eff}$ of the PS-LED is calculated according to Eq.(3)

$$\xi_{eff} = \frac{1}{2\pi} \frac{EDC}{4\, F_d\, d_{bd}} = \frac{1}{2\pi} \cdot \frac{\mu_D - 1}{\mu_D} \tag{3}$$

where $\mu_D = d_{bd}/d_y$ is the damper ductility.

## 3 EXPERIMENTAL CAMPAIGN

This paragraph presents the results of the experimental campaign conducted on two prototypes of PS-LED with the properties reported in Table 1. The design axial force was calculated in accordance with Eq.(1) in this paper assuming a shear stress at the interface $\tau_d$ = 0.112 · $p_d$, where $p_d$ is the design value of the axial prestress. In accordance with the requirements of the European standard [23] and assuming the worst scenario for displacement demand, the prototypes were constructed to accommodate an amplified displacement, in either direction, of $\gamma_x \cdot \gamma_b \cdot d_{bd}$, with $\gamma_b$ = 1.1 and $\gamma_x$ = 1.2. The equivalent viscous damping ratio $\xi_{eff}$ is dependent on the ductility factor $\mu_D$ according to Eq.(3).

| Prototype | $D$ [mm] | $L_c$ [kN] | $D_c$ [mm] | $d_{bd}$ [mm] | $\mu_D$ [%] | $p_d$ [MPa] | $F_d$ [kN] | $\xi_{eff}$ [%] |
|---|---|---|---|---|---|---|---|---|
| PS-LED 225/10 | 28.1 | 90 | 69.8 | 10 | 8 | 240 | 225 | 55.7 |
| PS-LED 50/15 | 20 | 70 | 69.8 | 15 | 30 | 100 | 52 | 61.4 |

**Table 1:** Dimensions of lead core, axial prestress and design properties of tested prototypes

The tests were conducted at the Material Testing Laboratory of Politecnico di Milano, using a servohydraulic Universal Testing Machine (MTS Systems, Eden Prairie, MN, USA) with a capacity of 500 kN. The axial prestress applied to the lead core was controlled by adjusting the tightening torque of the screws used to fix the container cap to the cylinder.

Figure 2 reports the results of the two prototypes tested for 10 cycles at $d_{bd}$ and frequency 0.5 Hz. The graphs show that, excluding the first cycle, which is affected from the static friction at the breakaway, the friction force remains stable at the design value associated with dynamic friction throughout all cycles, resulting in an almost rectangular hysteresis loop. In particular, the equivalent viscous damping ratio at $d_{bd}$ is 55.3% for the PS-LED 225/10 and 59.6% for the PS-LED 50/10, in good agreement with the design values (Table 1).

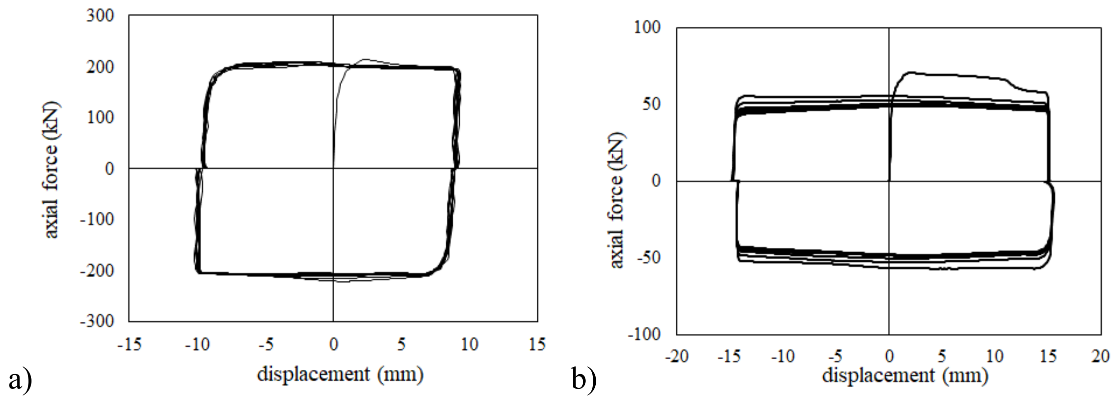


**Figure 2:** Experimental cyclic force – displacement curves of PS-LED prototypes: (a) PS-LED 225/10; (b) PS-LED 50/15

Figure 3 reports the results in terms of equivalent viscous damping ratio of the prototypes conducted at different velocities, confirming the stability of the response and the robustness of the device.

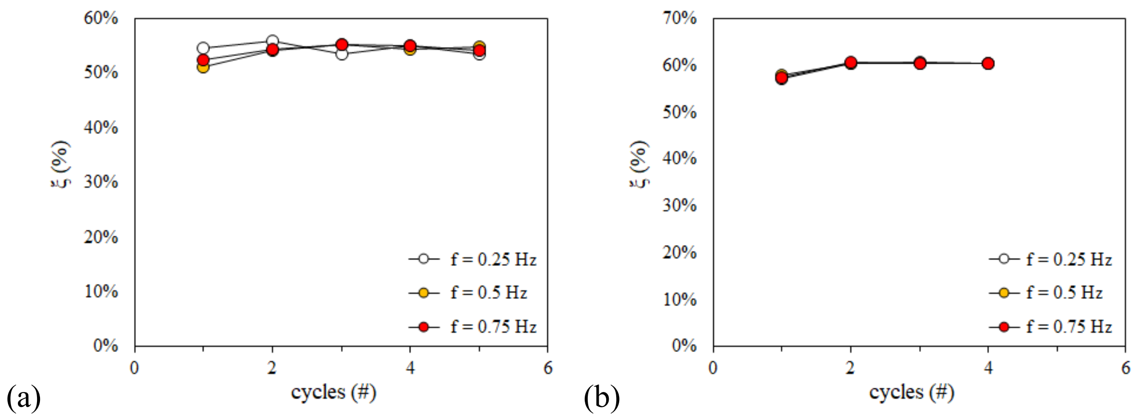


**Figure 3:** Equivalent viscous damping ratio of PS-LED 225/10 (a) and PS-LED 50/15 (b)

Figure 4 shows the response in terms of output force of the two devices during the final tests (stability tests) conducted to check the capacity of the device to resist multiple earthquakes without getting damaged. The stability tests, which are not contemplated in the European norm [23], consisted in three sequences of 10 cycles with amplitude equal to $d_{bd}$, with a dwell period of less than 2 hours between two consecutive sequences. Disregarding the response at the first cycle of each sequence, the maximum deviations of the output force from the experimental values assessed at the third cycle of the first sequence are less than 10%.

These results further confirm the robustness of the device and its ability to withstand multiple design level excitations without damaging.

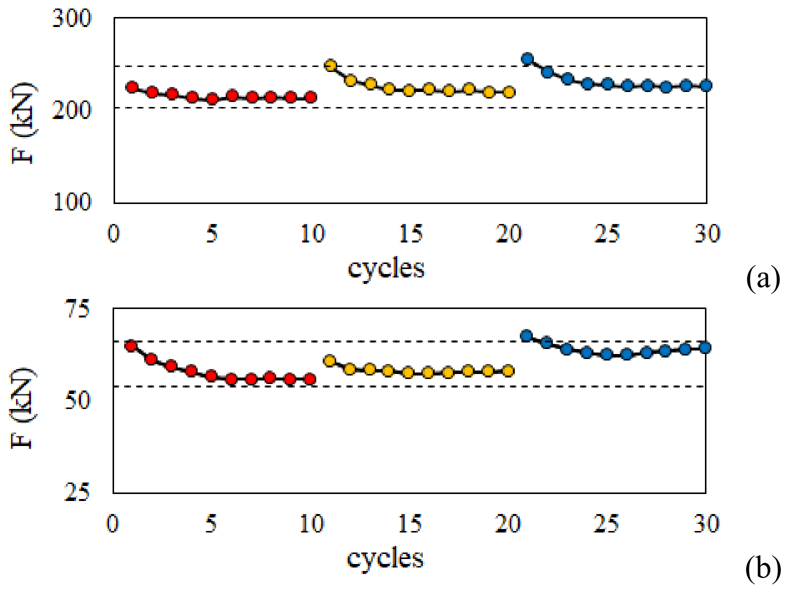


**Figure 4:** Axial force of PS-LED 225/10 (a) and PS-LED 50/15 (b) in the stability tests (dotted lines represent the +/-10% deviation from the values at the third cycle of the first sequence)

## 4 NUMERICAL INVESTIGATION IN OPENSEES

### 4.1 Retrofit design of the case-study structure

The structure considered as a case-study is a reinforced concrete (RC) building of residential use, already studied in the literature [24]-[27], whose geometry is reported in Figure 5. For sake of brevity, the details regarding materials and reinforcement are omitted; further information on all properties can be found in the relevant publications [24]-[27].

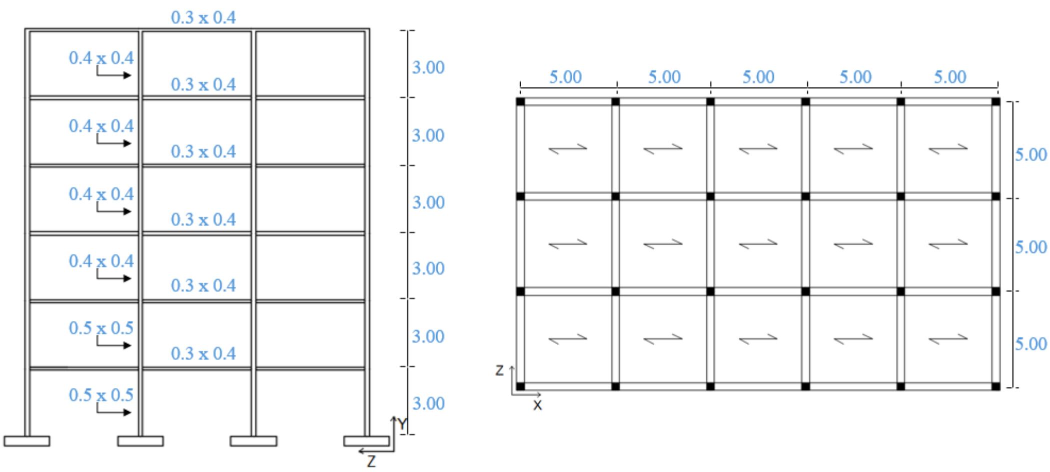


**Figure 5:** Elevation and plan view of the case-study building (dimensions in meters)

The building was designed according to the Italian Building Code [28] considering a moderate seismicity area characterized by PGA = 1.91 m/s$^2$ and soil type B, for a low ductility class (Class B), and is now retrofitted to withstand seismic action effects corresponding to a high seismic area with PGA = 2.26 m/s$^2$ and soil type C.

The retrofit design is performed by applying the Direct Displacement-Based Design (DDBD) retrofit procedure developed by some Authors of this work [25],[29] with the goal of guaranteeing that the structure is immediately accessible after a main earthquake. Diagonal steel braces equipped with hysteretic dampers, either PS-LED or BRB, are installed on the facades of the buildings according to the layout shown in Figure 6. For the PS-LED a ductility $\mu_D$ = 20 ($\xi_{eff}$ = 60.5%) is assumed, while the ductility of the BRB is equal to $\mu_D$ = 10 (with $\xi_{eff}$ almost equal to 30-40%) in agreement with other studies [21],[22]. With the goal of concentrating the largest part of the deformation of the story in the damper, enhancing the amount of energy dissipation, the stiffness associated to the steel brace $K_B$ is set to be $\geqslant$ 2 that of the damper $K_D$.

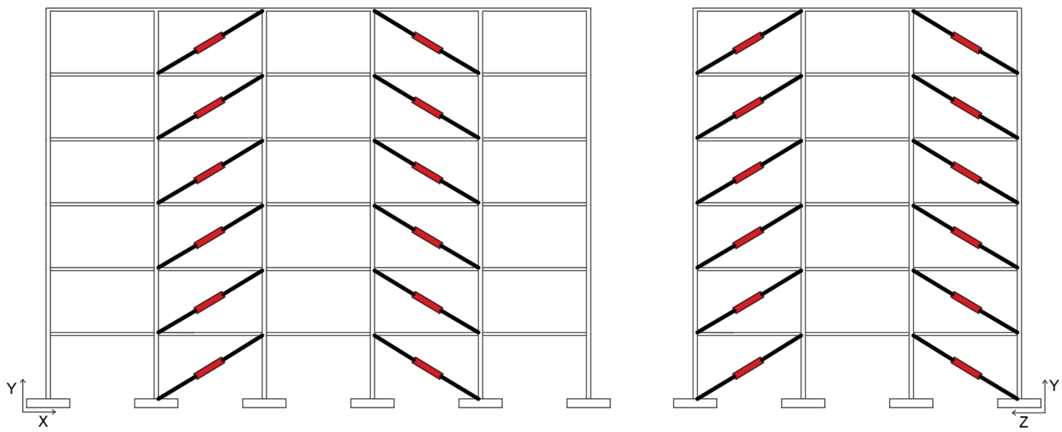


**Figure 6:** Layout of the diagonal steel braces equipped with hysteretic dampers installed in the case-study structure

## 4.2 Numerical model in OpenSees

The time history analyses are conducted using the OpenSees framework [30],[31], where a complete 3D numerical model of the structure is developed. Beams and columns are modeled with the *forceBeamColumn* element object [31], utilizing the *beamWithHinges* element [32]. This element is characterized by a linear elastic material behavior in the internal sub-element and a nonlinear behavior in the two outer sub-elements. The length of the plastic hinge, denoted as $L_{pl}$, is determined based on Eq. (A.9) of Eurocode 8 [33], using a well-defined concrete confinement model [34] (see Eq. (A.6) to (A.8) of Eurocode 8 [33]). A fiber section model is implemented, where the uniaxial *Concrete04* material, based on Popovics' model [35], is used for the nonlinear behavior of concrete, which is assumed to have no tensile strength. The *Steel02* material model, based on the Giuffre-Menegotto-Pinto law with isotropic strain hardening, is assigned to each steel bar represented by a fiber [36],[37]. An effective area moment of inertia $I_{eq}$, equal to 50% of the gross moment of inertia $I_g$, is assigned to the interior elastic sub-element, in accordance with both Italian and European standards [28],[33].

Masses corresponding to all structural elements (beams, columns, and slabs) are concentrated at the center of mass of each floor, while dead and live loads are uniformly distributed across the beams based on the tributary area method. P-Delta effects are accounted for, but bond slip and low-cycle fatigue effects are neglected, as the structure is designed to fail in flexure. Fixed base supports simulate rigid foundations at the columns on the ground floor. The Rayleigh method is used to define the damping of the frame, based solely on the tangent stiffness matrix, with a 5% viscous damping ratio. This method also considers the energy dissipation from infill panels and other non-structural elements [34].

The floor slabs are modeled as rigid diaphragms, with all nodes at each floor constrained to move together. 'Axial buffers' [38] are placed between the ends of beams and the adjacent nodes connected to the rigid diaphragm, using *zeroLength* element objects [31] with minimal axial stiffness. These buffers prevent fictitious axial forces arising from the interaction between beam elements modeled with fiber sections and the rigid diaphragm [38].

Each diagonal brace consists of a steel brace and a hysteretic damper in series. The steel brace is designed to behave elastically under design loads and is modeled as an *elasticBeamColumn* element [31]. This modeling approach provides a more accurate representation of the damped brace response, as the hysteretic behavior is localized only in the device element [15]. The PS-LED is modeled using a *truss* element object [31], with its constitutive behavior described by the EPPV (Elastic Perfectly Plastic and Viscous damper material) model introduced in [1] and summarized in Figure 7. The BRB behavior is captured using the uniaxial material model proposed by Zona and Dall'Asta [39], known as *SteelBRB*, which accounts for both kinematic and isotropic hardening as well as tension–compression asymmetry. The model parameters are based on the recommendations of [13]. This model is particularly effective in capturing the asymmetric tension-compression response typical of BRB devices.

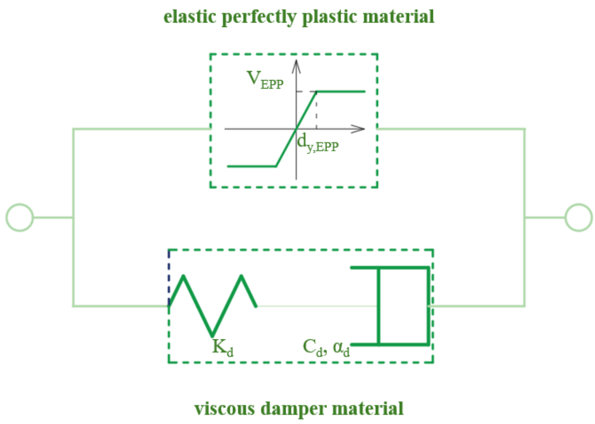


**Figure 7:** The EPPV model of the PS-LED [1]

## 4.3 Seismic input

Nonlinear dynamic analyses are performed using a set of 7 independent bidirectional natural ground motion records, sourced from the European Ground Motion Database [40] and selected via the Rexel software [41].

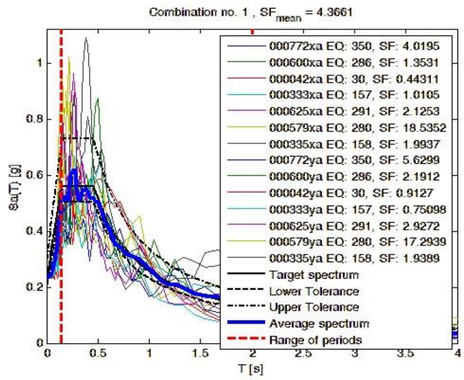


**Figure 8:** Scaled ground motion spectra and target spectra for the municipality of Arezzo and return period $T_R$=475 years. SF: scale factor

The seismic input is defined based on the Italian Building Code [28] provisions for the municipality of Arezzo, considering soil type C and seismic category $T_1$. The analyses focus on the life safety limit state, corresponding to a 10% probability of exceedance over the reference period $V_R$, which translates to a design earthquake with a return period $T_R$ of 475 years. Further details on the ground motion selection are illustrated in Figure 8 and Table 2. To incorporate potential directionality effects, each bidirectional earthquake record is applied in two separate analyses, swapping the excitation components along the primary structural axes.

| Earthquake Name | Mw | Fault Mechanism | Epicentral Distance [km] | PGA_X [m/s$^2$] | PGA_Z [m/s$^2$] | EC8 Site class |
|---|---|---|---|---|---|---|
| Umbria Marche (aftershock) | 5.3 | normal | 20 | 0.5673 | 0.405 | C |
| Umbria Marche | 6 | normal | 22 | 1.6852 | 1.0406 | C |
| Ionian | 5.8 | thrust | 15 | 5.1459 | 2.4983 | C |
| Alkion | 6.6 | normal | 20 | 2.2566 | 3.0363 | C |
| Umbria Marche (aftershock) | 5.5 | normal | 20 | 1.0729 | 0.779 | C |
| Gulf of Corinth | 5.3 | normal | 19 | 0.123 | 0.1318 | C |
| Alkion | 6.3 | normal | 25 | 1.1437 | 1.176 | C |

**Table 2:** Information about the selected natural ground motions

## 4.4 Results and discussion

The performance comparison between the structure retrofitted with PS-LED and that with BRB is based on key engineering demand parameters, including peak displacement (*d*), peak absolute acceleration (*a*), and maximum internal forces (axial force *N* and shear force *V*) in the columns connected to the damped braces.

Figure 9 illustrates the maximum displacements and the maximum absolute accelerations at each floor in X-direction. For brevity, results for the Z-direction are not included; however, the observations discussed in this paragraph remain generally applicable.

Figure 9(a) confirms that the PS-LED effectively controls structural displacements to a degree comparable to the BRB. In fact, in both directions, the displacement at the top floor aligns with the target design displacement $d_p$.

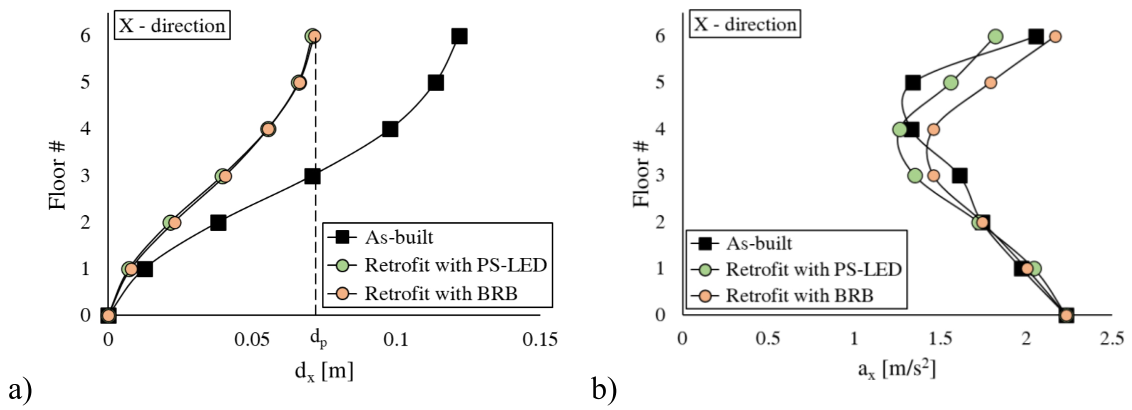


**Figure 9:** Maximum displacement and maximum absolute acceleration at each floor in X-direction

Notable differences between the two retrofitting strategies emerge in terms of absolute acceleration, as depicted in Figure 9(b). The structure equipped with PS-LED experiences acceleration levels generally similar to those of the as-built configuration and, in certain cases, such as the 3rd and 6th floors, even lower (by approximately 16% at the 3rd floor in the X-direction and 11% at the 6th floor in both directions). In contrast, the BRB-retrofitted structure exhibits higher acceleration values, particularly at the 4th, 5th, and 6th floors. This discrepancy stems from the greater energy dissipation capacity of the PS-LED, which achieves an equivalent viscous damping ratio about 60% higher than that of the BRB.

Figure 10 presents the axial force (*N*) and shear force (*V*) in X-direction at each floor, averaged over all columns connected to the damped braces, as per the configuration shown in Figure 6. The overall trend is similar for both retrofitting solutions, with an increase in axial force (*N*) in the lower floors (1st and 2nd) and a reduction in shear forces (*V*) compared to the as-built structure. However, the increase in axial force is less pronounced in the PS-LED system (+26% at the ground floor, compared to +37% in the BRB case). Likewise, regarding shear forces (*V*), the PS-LED achieves a reduction of over 20% in the X-direction, whereas the BRB achieves approximately 10%.

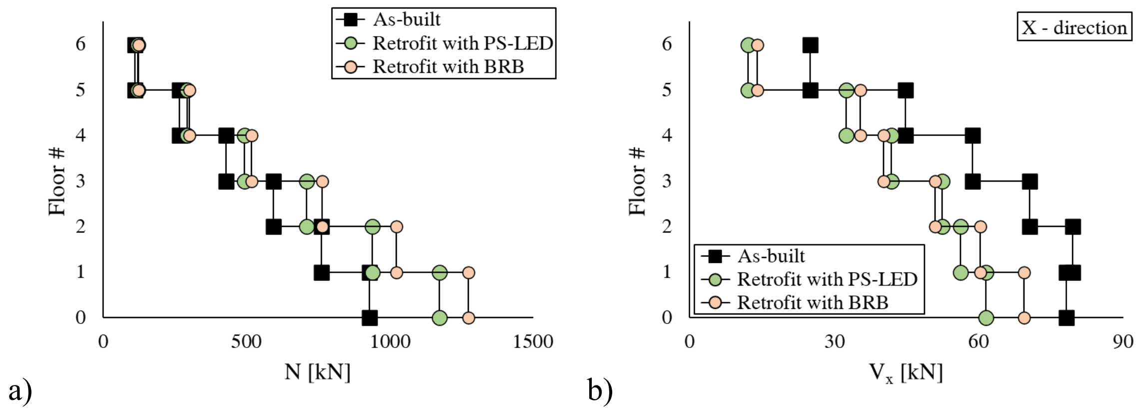


**Figure 10**: Maximum average axial force (a) and shear force in X-direction (b) in the pillars of ground floor

## 5 CONCLUSIONS

The study investigates the PreStressed LEad Damper (PS-LED), a hysteretic friction damper with valuable technical characteristics, such as the insensitivity to fatigue, the ability to accommodate multiple design strong motions without being damaged, a high stiffness and a high damping capability. The PS-LED was first introduced in [2], where a first device was initially tested. The present contribution extends the experimental campaign to a second prototype with different properties, useful to validate the conceptual design presented herein.

Additionally, a numerical analysis is conducted on a case-study structure, retrofitted with diagonal steel braces equipped with either the PS-LED or a conventional Buckling Restrained Brace (BRB), to highlight the advantages of the PS-LED over the state-of-the-art device. Even if the numerical modeling of the damper was already introduced in [1], the model in this manuscript has been enhanced to account for the in-series contribution of the damper and the steel brace used to insert the damper into the structure. Moreover, a direct comparison with the BRB, modeled according to established literature, has never been studied.

Bidirectional non-linear dynamic analyses are conducted, and the results of the new study demonstrate that the PS-LED significantly enhances energy dissipation capabilities, resulting in notable reductions in floor accelerations and shear forces impacting the columns of the structure when compared to the BRB. These outcomes underscore the PS-LED's potential to improve seismic resilience, presenting a viable alternative to traditional damping technologies.

## REFERENCES

[1] Bruschi, E., Quaglini, V., 2022. Assessment of a novel hysteretic friction damper for the seismic retrofit of reinforced concrete frame structures. Structures 46, 793–811. https://doi.org/10.1016/j.istruc.2022.10.113.

[2] Quaglini, V., Pettorruso, C., Bruschi, E., 2022. Design and Experimental Assessment of a Prestressed Lead Damper with Straight Shaft for Seismic Protection of Structures. Geosciences (Switzerland) 12. https://doi.org/10.3390/geosciences12050182.

[3] Bruschi, E., Zoccolini, L., Cattaneo, S., Quaglini, V., 2023. Experimental Characterization, Modeling, and Numerical Evaluation of a Novel Friction Damper for the Seismic Upgrade of Existing Buildings. Materials 16. https://doi.org/10.3390/ma16051933.

[4] Freddi, F., Ghosh, J., Kotoky, N., Raghunandan, M., 2021. Device uncertainty propagation in low-ductility RC frames retrofitted with BRBs for seismic risk mitigation. Earthquake Engineering & Structural Dynamics 50, 2488–2509. https://doi.org/10.1002/eqe.3456.

[5] Watanabe, A., 2018. Design and Applications of Buckling-Restrained Braces. International Journal of High-Rise Buildings 7, 215–221. https://doi.org/10.21022/IJHRB.2018.7.3.215.

[6] Tsai, K. C., Lai, J. W., Hwang, Y. C., Lin, S. L., Weng, C. H., 2004. Research and application of double-core Buckling-restrained Braces in Taiwan, 13th World Conference on Earthquake Engineering Vancouver, B. C., Canada August 1-6, Paper No. 2179.

[7] Wada, A., Takeuchi, T., 2017. Buckling-Restrained Braces and Applications, The Japan Society of Seismic Isolation, Chapter 1.

[8] Wada, A., Takeuchi, T., 2017. Buckling-Restrained Braces and Applications, Chapter 7., The Japan Society of Seismic Isolation.

[9] Watanabe, A., Hitomi, Y., Saeki, E., Wada, A., Fujimoto, M., 1988. Properties of brace encased in buckling-restraining concrete and steel tube, 9WCEE, Vol. IV, pp. 719724, JADP, Tokyo, Japan.

[10] Freddi, F., Tubaldi, E., Zona, A., Dall'Asta, A., 2021. Seismic performance of dual systems coupling moment-resisting and buckling-restrained braced frames. Earthquake Engineering & Structural Dynamics 50, 329–353. https://doi.org/10.1002/eqe.3332.

[11] Gutiérrez-Urzúa, F., Freddi, F., 2022. Influence of the design objectives on the seismic performance of steel moment resisting frames retrofitted with buckling restrained braces. Earthquake Engineering & Structural Dynamics 51, 3131–3153. https://doi.org/10.1002/eqe.3717.

[12] Barbagallo, F., Bosco, M., Marino, E.M., Rossi, P.P., Stramondo, P.R., 2017. A multi‐performance design method for seismic upgrading of existing RC frames by BRBs. Earthq Engng Struct Dyn 46, 1099‐1119. https://doi.org/10.1002/eqe.2846.

[13] Bosco, M., Marino, E.M., Rossi, P.P., 2015. Design of steel frames equipped with BRBs in the framework of Eurocode 8. Journal of Constructional Steel Research 113, 43–57. https://doi.org/10.1016/j.jcsr.2015.05.016.

[14] Barbagallo, F., Bosco, M., Marino, E.M., Rossi, P.P., 2019. Seismic design and performance of dual structures with BRBs and semi-rigid connections. Journal of Constructional Steel Research 158, 306–316. https://doi.org/10.1016/j.jcsr.2019.03.030.

[15] Castaldo, P., Tubaldi, E., Selvi, F., Gioiella, L., 2021. Seismic performance of an existing RC structure retrofitted with buckling restrained braces. Journal of Building Engineering 33, 101688. https://doi.org/10.1016/j.jobe.2020.101688.

[16] Sonda, D., Pollini, A., Cossu, M., 2019. Seismic Retrofit of an Industrial Building Using Damping Devices, Structural Engineering International. DOI: 10.1080/10168664.2019.1635975.

[17] Zerbin, M., Aprile, Al., Dalmonte, C., Sereni, A., Zoli, M., Ugatti, A., 2023. Seismic Retrofit of a Precast RC School Building with External BRBs in Northen Italy. fib Symposium, pp. 170-179. DOI: 10.1007/978-3-031-32511-3_19.

[18] Di Sarno, L., Manfredi, G., 2010. Seismic retrofitting with buckling restrained braces: Application to an existing non-ductile RC framed building. Soil Dynamics and Earthquake Engineering 30, 1279–1297. https://doi.org/10.1016/j.soildyn.2010.06.001.

[19] Antonucci, R., Balducci, F., Castellano, M.G., Donà, F., 2006. Pre-casted RC buildings with Buckling Restrained Braces: the example of the new building of the faculty of engineering in Ancona. Second International fib Congress, Napoli, Italy, June 5-8, 2006, paper No. 879.

[20] Watanabe, A., 2018. Design and Applications of Buckling-Restrained Braces. International Journal of High-Rise Buildings 7, 215–221. https://doi.org/10.21022/IJHRB.2018.7.3.215.

[21] Nuzzo I, Losanno D, Caterino N. Seismic design and retrofit of frames structures with hysteretic dampers: a simplified displacement-based procedure. Bull Earthq Eng 2019;17:2787-2819. DOI: 10.1007/s10518-019-00558-8.

[22] Gandelli E, Taras A, Disti J, Quaglini V. Seismic retrofit of hospitals by means of hysteretic braces: influence on acceleration-sensitive non-structural components. Front Built Environ 2019;5(100). DOI: doi.org/10.3389/fbuil.2019.00100.

[23] CEN (European Committee for Standardization). European Committee for Standardization (2009). EN 15129. Anti-seismic devices. Brussels.

[24] Faleschini, F., Zanini, M.A., Toska, K., 2019. Seismic reliability assessment of code-conforming reinforced concrete buildings made with electric arc furnace slag aggregates. Engineering Structures 195, 324–339. https://doi.org/10.1016/j.engstruct.2019.05.083.

[25] Bruschi, E., Quaglini, V., Calvi, P.M., 2022. A simplified design procedure for seismic upgrade of frame structures equipped with hysteretic dampers. Engineering Structures 251. https://doi.org/10.1016/j.engstruct.2021.113504.

[26] Bruschi, E., Quaglini, V., 2024. Reliability analysis of two archetype RC buildings with hysteretic dampers. Soil Dynamics and Earthquake Engineering 176. https://doi.org/10.1016/j.soildyn.2023.108290.

[27] Bruschi, E., Quaglini, V. 2024. Assessment of Non-Linear Analyses of RC Buildings Retrofitted with Hysteretic Dampers According to the Italian Building Code. Appl. Sci. 2024, 14, 2684. https://doi.org/10.3390/app14072684.

[28] CSLLPP (Consiglio Superiore dei Lavori Pubblici). D.M. 17 gennaio 2018 in materia di "norme tecniche per le costruzioni". Gazzetta ufficiale n.42 del 20 febbraio 2018, Supplemento ordinario n.8, Ministero delle Infrastrutture e dei trasporti, Roma; 2018, in Italian.

[29] Bruschi, E., Quaglini, V., Zoccolini, L., 2023. Seismic Upgrade of Steel Frame Buildings by Using Damped Braces. Applied Sciences (Switzerland) 13. https://doi.org/10.3390/app13042063.

[30] McKenna F, Fenves GL, Scott MH. Open System for Earthquake Engineering Simulation, PEER Report, Berkeley, CA; 2000.

[31] OpenSeesWiki online manual. Available online at: https://opensees.berkeley.edu/wiki/index.php/Main_Page.

[32] Scott MH, Fenves GL. Plastic Hinge Integration Methods for Force-Based Beam-Column Elements. J Struct Eng 2006;132(2):244-252. DOI: 10.1061/(ASCE)0733-9445(2006)132:2(244).

[33] CEN (European Committee for Standardization). Design of structures for earthquake resistance – Part 3: Assessment and retrofitting of buildings. EN 1998–3 Eurocode 8; 2005.

[34] Bruschi E, Calvi PM, Quaglini V. Concentrated plasticity modelling of RC frames in time-history analyses. Eng Struct 2021;243:112716. DOI: 10.1016/j.engstruct.2021.112716.

[35] Popovics S. A numerical approach to the complete stress-strain curve of concrete. Cem Concr Res 1973;3(5):583-599.

[36] Menegotto M, Pinto PE. Method of analysis for cyclically loaded RC plane frames including changes in geometry and non-elastic behaviour of elements under combined normal force and bending. IABSE: Symposium on resistance and ultimate deformability of structures acted on by well defined repeated loads 1973 – Final Report.

[37] Filippou FC, Popov EP, Bertero VV. Effects of Bond Deterioration on Hysteretic Behavior of Reinforced Concrete Joints, Report EERC 83-19, Earthquake Engineering Research Center, University of California, Berkeley, 1983.

[38] Barbagallo, F., Bosco, M., Marino, E., Rossi, P., 2020. On the fibre modelling of beams in RC framed buildings with rigid diaphragm. Bull Earthq Eng18:189-210. DOI: 10.1007/s10518-019-00723-z.

[39] Zona, A., Dall'Asta, A., 2012. Elastoplastic model for steel buckling-restrained braces. Journal of Constructional Steel Research 68, 118–125. https://doi.org/10.1016/j.jcsr.2011.07.017.

[40] Ambraseys N, Smit P, Sigbjornsson R, Suhadolc P, Margaris B. Internet-Site for European Strong-Motion Data, European Commission, Research-Directorate General, Environment and Climate Programme, 2002.

[41] Iervolino I, Galasso C, Cosenza E. REXEL: computer aided record selection for code-based seismic structural analysis. Bull Earthq Eng 2010;8:339-362. https://doi.org/10.1007/s10518-009-9146-1.